



HAL
open science

Infrasound modeling in a spherical heterogeneous atmosphere

J.-X. Dessa, J. Virieux, S. Lambotte

► **To cite this version:**

J.-X. Dessa, J. Virieux, S. Lambotte. Infrasound modeling in a spherical heterogeneous atmosphere. Geophysical Research Letters, 2005, 32, pp.L12808. 10.1029/2005GL022867 . insu-00355221

HAL Id: insu-00355221

<https://insu.hal.science/insu-00355221>

Submitted on 19 Feb 2021

HAL is a multi-disciplinary open access archive for the deposit and dissemination of scientific research documents, whether they are published or not. The documents may come from teaching and research institutions in France or abroad, or from public or private research centers.

L'archive ouverte pluridisciplinaire **HAL**, est destinée au dépôt et à la diffusion de documents scientifiques de niveau recherche, publiés ou non, émanant des établissements d'enseignement et de recherche français ou étrangers, des laboratoires publics ou privés.

Infrasound modeling in a spherical heterogeneous atmosphere

J.-X. Dessa,^{1,2} J. Virieux,¹ and S. Lambotte³

Received 1 March 2005; revised 2 May 2005; accepted 23 May 2005; published 21 June 2005.

[1] The deployment of a worldwide network for infrasound detection requires numerical methods for modeling these signals over long distances. A ray theoretical approach appears robust and efficient. It furthermore allows a straightforward interpretation of recorded phases. We have developed a three-dimensional Hamiltonian ray tracing for modeling linear acoustic waves in the atmosphere. Propagating over distances superior to 500 km requires the curvature of the Earth to be considered, which is achieved by using spherical coordinates. High atmospheric winds are properly handled through a modified Hamiltonian. These winds as well as sound velocity can change significantly during long-lasting propagations; these variations are also included in our modeling. Finally, the amplitude of infrasonic signals is computed by concomitantly solving for paraxial rays and assessing the evolution of the ray tube thus defined. We present the theory for this atmospheric infrasound modeling and some simple applications that establish its robustness and potential. **Citation:** Dessa, J.-X., J. Virieux, and S. Lambotte (2005), Infrasound modeling in a spherical heterogeneous atmosphere, *Geophys. Res. Lett.*, *32*, L12808, doi:10.1029/2005GL022867.

1. Introduction

[2] An international detection network dedicated to the control of the Comprehensive Test Ban Treaty (CTBT) over the entire Earth is being deployed. Infrasonic waves of various origins are recorded by these stations and fast acoustic propagation tools over the 200-km thick, spherical atmosphere are required to model these signals. Atmospheric winds are very strong (up to $100 \text{ m}\cdot\text{s}^{-1}$) along the East-West direction in the stratosphere and mesosphere, and along the North-South direction in the thermosphere (Figure 1). These winds are not negligible compared to the sound velocity. Therefore, they may modify significantly the wave propagation and the resulting ray paths, travel times and amplitudes, recorded at ground-based micro-barometric stations [Virieux *et al.*, 2004]. Furthermore, daily to seasonal variations are observed for these winds as well as for the sound velocity. These observations—based on radar, balloons, satellites experiments etc.—help construct global databases for spatial and temporal descriptions of the wind and sound velocity distributions in the atmosphere [Hedin, 1991; Hedin *et al.*, 1991, 1996]. Taking these variations into

account is essential for an accurate modeling of long-range infrasound propagation.

[3] Complete solutions based on numerically demanding fluid mechanics tools are of little use in an operating context where the rapidity for discriminating infrasound sources is a crucial issue. Asymptotic wave propagation therefore appears as an elegant competitive approach that however theoretically reduces the modeling to signals above ~ 5 Hz, out of the range of gravity waves; numerous natural or artificial sources (e.g. volcanic eruptions, explosions) radiate significant energy in this validity range.

[4] Ray-based modeling of infrasound propagation has already been achieved for 1D layered structures [Garcés *et al.*, 1998] and for 2D cartesian ones [Virieux *et al.*, 2004]. In the approach of Virieux *et al.* [2004], both ray trajectories (with corresponding travel times) and amplitudes are computed and the caustics are detected [Abdullaev, 1993]. We present here the extension of this approach to 3D spherical, non stationary structures in order to handle the Earth's curvature and the effect of time variations in the atmospheric properties during long-range modeling of infrasound propagation.

2. Ray Theory in a Moving Medium

2.1. Canonical Equations

[5] Pressure perturbations are assumed to be small so that the motion of the atmospheric medium follows linearized hydrodynamic equations for a compressible fluid. The high frequency approximation propagation introduces the Hamiltonian function \mathcal{H} [Burridge, 1976]. It is modified here in order to include the wind's effect [Abdullaev, 1993; Virieux *et al.*, 2004]:

$$\mathcal{H}(\mathbf{p}, \mathbf{q}) = \frac{1}{2} \left[\mathbf{p}^2 - \frac{1}{c_0(\mathbf{q})^2} (1 - \mathbf{p} \cdot \mathbf{v}(\mathbf{q}))^2 \right]. \quad (1)$$

The ray position is denoted by \mathbf{q} ; the slowness vector \mathbf{p} is normal to the wavefront and related to the travel time T along the ray by $\mathbf{p} = \nabla T$; the sonic velocity $c_0(\mathbf{q})$ is a scalar while the wind velocity $\mathbf{v}(\mathbf{q})$ is a vector.

[6] If atmospheric properties are allowed to vary during the time of propagation, then quantities c_0 , \mathbf{v} and \mathcal{H} depend explicitly on a variable of evolution ν and the general Hamilton-Jacobi equation is:

$$\mathcal{H}(\mathbf{p}, \mathbf{q}, \nu) + \frac{\partial T}{\partial \nu} = 0, \quad (2)$$

where dependence upon time is considered through the ray sampling parameter ν , mathematically defined below. Using

¹Géosciences Azur, UNSA, Valbonne, France.

²Now at Institut de Physique du Globe de Paris, Paris, France.

³EOST, Institut de Physique du Globe de Strasbourg, Strasbourg, France.

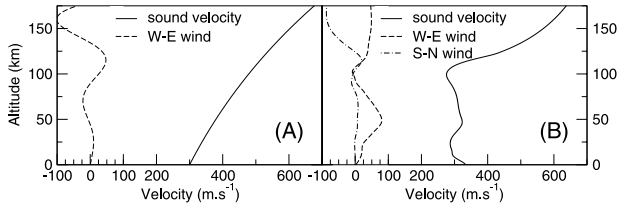


Figure 1. (A) Analytic atmospheric profiles (combined exponential and sinusoidal functions) used to compare cartesian and spherical kinematic ray tracing. (B) Atmospheric model used in the other tests presented. Winds blowing northward and eastward are positive.

analytical mechanics, canonical equations defining the ray in space and time are

$$\frac{d\mathbf{q}}{dv} = \nabla_{\mathbf{p}}\mathcal{H}, \quad \frac{d\mathbf{p}}{dv} = -\nabla_{\mathbf{q}}\mathcal{H}, \quad \frac{dT}{dv} = -\mathcal{H} + \mathbf{p} \cdot \nabla_{\mathbf{p}}\mathcal{H} \quad (3)$$

2.2. Ray Tracing in Spherical Coordinates

[7] Due to its sound velocity structure, the atmosphere predominantly behaves as a wave guide for infrasonic waves whose traveling distance can thus prove very large. It is therefore fundamental to take the Earth's curvature into account by using spherical coordinates. In a spherical reference frame attached to the Earth, a position is defined by its coordinates ρ , θ , and φ , denoting respectively the distance from the Earth's center, the colatitude—measured with respect to its S-N axis—and the longitude. Position and slowness vectors are defined by

$$\tilde{\mathbf{q}} = \begin{pmatrix} \rho \\ \rho\theta \\ \rho \sin\theta\varphi \end{pmatrix}, \quad \tilde{\mathbf{p}} = \begin{pmatrix} \dot{\rho}^{-1} \\ (\rho\dot{\theta})^{-1} \\ (\rho \sin\theta\dot{\varphi})^{-1} \end{pmatrix}. \quad (4)$$

[8] In a similar way, the vector $\tilde{\mathbf{v}}$ for wind velocity is introduced. The hamiltonian written in spherical coordinates is thus given by

$$\frac{1}{2} \left[\tilde{\mathbf{p}}^2 - \frac{1}{c_0(\mathbf{q}, \nu)^2} (1 - \tilde{\mathbf{p}} \cdot \tilde{\mathbf{v}}(\mathbf{q}, \nu))^2 \right]. \quad (5)$$

[9] The axis defined by $\theta = 0$ represents a singularity and, if the ray tracing equations are to be solved in the vicinity of the poles, an appropriate rotation of the reference frame must be preliminarily performed to avoid the singularity problem.

2.3. Numerical Integration

[10] The system (3) is solved by a second-order Runge-Kutta scheme with a finite integration step $\Delta\nu$ and initial conditions $\mathbf{q}(\nu = 0)$ and $\mathbf{p}(\nu = 0)$ defining the position of the source and the initial direction of the ray. The latter is defined in 3D by the azimuth of the ray with respect to the North and the dip angle with respect to the local vertical direction. For a given initial ray parameter, two dip angles at most should be considered, corresponding to initially upgoing and downgoing modes. These angles are complementary only if the vertical component of the wind is zero.

For a source on the ground, only the upgoing solution is meaningful.

[11] The atmospheric sound speed and wind velocities are sampled in time and space on a grid. During numerical integration, spatial interpolation at each point of the ray is done with 3rd order cardinal b-spline functions and time interpolation is done linearly. For real applications, space and time dependent models MSISE-90 and HWM-93 [Hedin, 1991; Hedin et al., 1991, 1996] can be used. These standard models only include horizontal winds. Note, however, that vertical winds could be considered at no extra-cost.

2.4. Amplitude Computation

[12] Considering small perturbations $\delta\mathbf{p}$ and $\delta\mathbf{q}$ around a central ray of reference, one can build neighboring paraxial rays. First order linearization of the system (3) yields [Farra and Madariaga, 1987]

$$\begin{pmatrix} \frac{\partial\delta\mathbf{q}}{\partial\nu} \\ \frac{\partial\delta\mathbf{p}}{\partial\nu} \end{pmatrix} = \begin{pmatrix} \nabla_{\mathbf{p}}\nabla_{\mathbf{q}}\mathcal{H} & \nabla_{\mathbf{p}}\nabla_{\mathbf{p}}\mathcal{H} \\ -\nabla_{\mathbf{q}}\nabla_{\mathbf{q}}\mathcal{H} & -\nabla_{\mathbf{q}}\nabla_{\mathbf{p}}\mathcal{H} \end{pmatrix} \begin{pmatrix} \delta\mathbf{q} \\ \delta\mathbf{p} \end{pmatrix}. \quad (6)$$

[13] While computing a ray, arbitrarily close rays defined through an initial perturbation can be propagated by solving this paraxial system. In 3D, two paraxial rays and the reference ray can thus define a ray tube whose cross-section is calculated. Practically, these two paraxial rays derive from three paraxial trajectories by linear combinations. The cross-section \mathcal{J} of the ray tube is then calculated (see Appendix A and complete algebra given by Virieux and Farra [1991]).

[14] Caustics are detected by sign changes of \mathcal{J} and are handled by incrementing k_{KMAH} , the so-called KMAH index [Chapman, 1985], and phase shifting the wave accordingly. Considering a constant energy flux in the ray tube and a variable density d , this yields the equation ruling the amplitude's evolution along the ray [e.g., Virieux et al., 2004]:

$$A(\nu_1) = A(\nu_0) \sqrt{\frac{c(\nu_1)d(\nu_1)\mathcal{J}(\nu_0)}{c(\nu_0)d(\nu_0)\mathcal{J}(\nu_1)}} e^{i k_{\text{KMAH}}\pi/2}, \quad (7)$$

with c the effective velocity of the wave (taking the wind into account).

[15] Atmospheric absorption by diffusion, visco-thermic and relaxation losses is not negligible for long thermospheric propagations. This effect can be introduced in the amplitude calculation through attenuation coefficients [Sutherland and Bass, 1996] that depend on the wave frequency and atmospheric properties (composition, temperature, pressure, density). Practically, mean attenuation profiles are computed, based on model MSISE-90. During the ray integration, they are linearly interpolated and yield a coefficient α . The amplitude is subsequently multiplied by $\exp(-\alpha\Delta l)$ where Δl is the length of the ray segment.

2.5. Rebound Conditions

[16] As explained before, infrasonic pressure waves are usually guided in the atmosphere and can periodically bounce on the ground. Care must be taken in computing

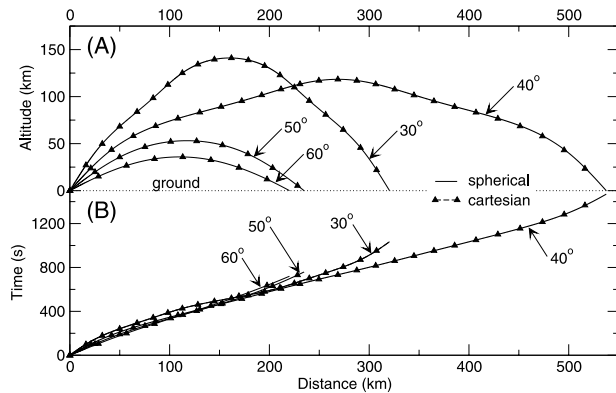


Figure 2. Rays obtained with our spherical ray tracing and a 3D extension of the code described by *Virieux et al.* [2004]; the propagation model has a spherical symmetry in each case. (A) Ray paths with labeled initial incidences. (B) Corresponding travel times.

these bounces. Considering a simple flat ground, bouncing conditions for the central ray are quite simple, the normal component being simply replaced by its opposite ($p_p^R = -pp^I$, where the superscripts I and R stand for the incident and reflected wave respectively) and the others remaining unchanged. Note that more complicated topographies make this condition more complex but could be easily taken into account. For paraxial rays, reflection conditions are somewhat more cumbersome to derive since the paraxial ray does not hit the ground at the same time and must be projected down to the ground before being reflected. Two operators \mathcal{P} and \mathcal{R} must therefore be applied, yielding:

$$\begin{pmatrix} \delta q^R \\ \delta p^R \end{pmatrix} = \mathcal{R}\mathcal{P} \begin{pmatrix} \delta q^I \\ \delta p^I \end{pmatrix}. \quad (8)$$

[17] The algebra for the calculation of \mathcal{P} and \mathcal{R} is given by *Farra et al.* [1989]. The expression of these operators in our case is given in Appendix B.

3. Validation of the Kinematic Ray Tracing

[18] A first test consists in validating our ray tracing in spherical coordinates by comparing its results with those independently obtained by a 3D extension of its cartesian equivalent, whose robustness is established [*Virieux et al.*, 2004]. For a given model of atmosphere, computed ray paths must be independent of the coordinate system in which ray tracing equations are solved. Therefore, the computations in cartesian and spherical coordinates should give the same result, provided that the atmosphere is described with the same symmetry for both modelings. Analytical sound velocity and wind profiles with roughly realistic variations are designed for this purpose, so that possible differences in the numerical interpolations do not affect the result. Only a zonal wind is considered, which is not limiting. An analytical, laterally invariant model of atmosphere is thus built (Figure 1a). It is either described on a cartesian or spherical modeling grid but has a spherical symmetry in both cases. Rays are shot from a ground-based source, towards East (Figure 2). The two sets of trajectories and travel times are practically indiscernible. The same level

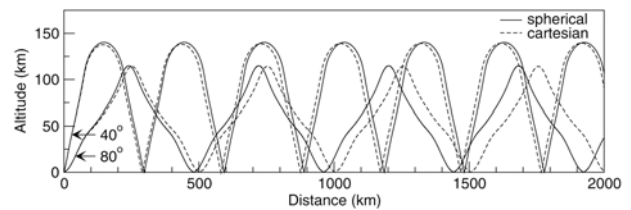


Figure 3. Rays obtained with the same 1D profiles considering either cartesian (flat Earth with horizontal distance) or spherical (curvilinear distance) symmetries.

of agreement is obtained for perpendicular directions of propagation (not presented here). The kinematic part of our ray tracing is thus proven to give compatible results.

[19] The Earth being considered as a sphere at first order, the natural parameterization of atmospheric models is a spherical coordinate system. Neglecting the Earth's curvature is only justified for short range propagations. At horizontal distances larger than about 500 km, inaccurate results may exceed both the intrinsic uncertainties of the modeling and the data precision. This is illustrated in Figure 3 where errors as large as ~ 100 km between corresponding rebound positions are observed after 2000 km of propagation. Unlike the preceding test, the modelings are performed in models whose symmetry correspond to the coordinate system in which equations are solved (cartesian or spherical). The vertical profiles of atmosphere used for this test and those presented hereafter are displayed in Figure 1b. Note again that, for simplicity, tests are carried out with this 1D, stationary model but that lateral and time variations can be considered as well.

4. Validation of the Dynamic Ray Tracing

[20] A simple test for the computation of wave amplitude is made by propagating over a long range in a homogeneous model and checking that the solution matches the simple

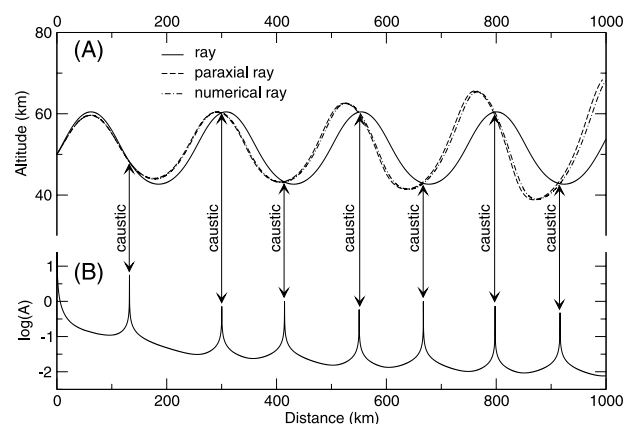


Figure 4. (A) Ray path for a westward propagation (source altitude: 50 km, initial incidence: 80°). The in-plane paraxial ray and a neighboring ray computed independently by slightly varying the initial incidence are also represented with artificial amplification of differences; they cross the reference ray coincidentally at caustics. (B) Amplitude of the pressure wave along the central ray; the singularities correlate exactly with caustics.

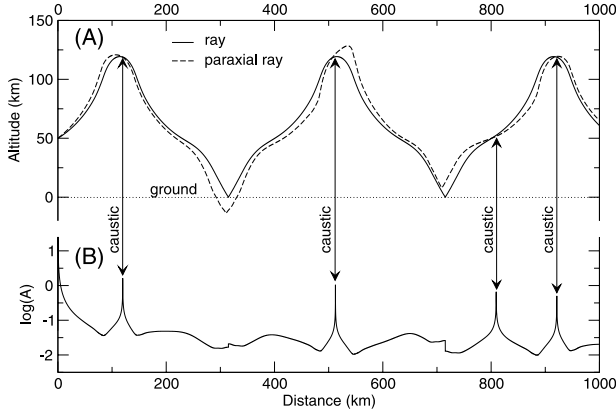


Figure 5. Same as in Figure 4 except for an eastward propagation and an initial incidence of 70° . Periodical rebounds on the ground are observed and here again, amplitude singularities correlate with caustics.

analytic solution, inversely proportional to the distance; agreement to within a range of 4.2% is found after 1500 km.

[21] For realistic velocity models, the focusing and defocusing effects of the ray tube can be surveyed by checking the coincidence between singularities of the computed amplitude and the existence of caustics at which neighboring rays cross each other. These crossing rays can be either two very close rays or a ray and a paraxial ray [Virieux *et al.*, 2004]. Two such tests are presented in Figures 4 and 5. Depending on the initial incidence and direction with respect to the wind, the ray is either totally guided in the atmosphere (with upper and lower refraction altitudes) or experiences periodic rebounds on the ground. In both cases, one can verify the correlation between caustics and amplitude singularities. The second example moreover validates our rebound conditions for paraxial rays as the correlation can still be observed after rebounds, thanks to the paraxial reflection conditions. In these two examples, only the in-plane paraxial ray yields caustics, the other one moving increasingly away from the central ray in a 1D atmosphere.

5. Conclusions

[22] Thanks to the Hamiltonian formulation, ray tracing in a moving atmosphere can be performed quite simply and efficiently. Spherical geometry is taken into account and proper conditions for rebounds on the ground of rays and paraxial rays have been applied for a spherical topography. Amplitude exhibits bright spots related to ray focusing in the atmospheric wave guide. One may detect these features with a global micro-barometric network of sufficient density. Amplitude decay with distance could be corrected and the source estimation and discrimination should be possible. Furthermore, tomographic approaches based on such modeling could be developed in order to improve atmospheric models and to provide a large-scale complement to existing means of in situ measurement, in the same way as what is routinely done for investigating the deep solid earth by seismic or seismological methods.

[23] Due to the exponential decay of the atmospheric density with altitude, the assumption of small pressure perturbation by the propagating signal on which the

present study is based may not be verified for powerful sources and non linear shock waves may occur. In that case, the propagation velocity does not only depend on the local atmospheric properties but also on the amplitude of the wave itself [e.g., Besset and Blanc, 1994]. Here, paraxial ray tracing is proven to be capable of modeling amplitudes along ray fields in a complex varying atmosphere. Therefore, this approach makes possible addressing the problem of non-linear acoustic propagation in complex models of atmosphere. This is a clear direction for future developments.

Appendix A: Ray Tube Cross-Section

[24] Three paraxial trajectories are defined with initial perturbations $\delta\tilde{\mathbf{p}}^{\tau_j} = (\delta_{j,k})_{k \in [1,3] \equiv [p, \theta, \varphi]}$, (with $\delta_{j,k}$ the Kronecker symbol), from which two paraxial rays $\pi_{1,2}$ are built:

$$\begin{aligned} \delta\tilde{\mathbf{w}}^{\pi_1}(\nu) &= \hat{p}_{\varphi_1} \delta\tilde{\mathbf{w}}^{\tau_2}(\nu) - \hat{p}_{\theta_1} \delta\tilde{\mathbf{w}}^{\tau_3}(\nu), \\ \delta\tilde{\mathbf{w}}^{\pi_2}(\nu) &= \hat{p}_{\varphi_1} \delta\tilde{\mathbf{w}}^{\tau_1}(\nu) - \hat{p}_{\theta_1} \delta\tilde{\mathbf{w}}^{\tau_3}(\nu); \end{aligned} \quad (\text{A1})$$

with $\delta\tilde{\mathbf{w}} = (\delta\tilde{\mathbf{q}}, \delta\tilde{\mathbf{p}})$ and $\hat{p}_{\rho_i}, \hat{p}_{\theta_i}, \hat{p}_{\varphi_i}$ dimensionless scalars proportional to the initial slowness vector's components. The central ray and the two paraxial rays define a tube whose cross-section is proportional to [Virieux and Farra, 1991]:

$$\mathcal{J} = \begin{vmatrix} \tilde{p}_\rho & \delta\tilde{\mathbf{q}}_p^{\tau_1} & \delta\tilde{\mathbf{q}}_p^{\tau_2} & \delta\tilde{\mathbf{q}}_p^{\tau_3} \\ \tilde{p}_\theta & \delta\tilde{\mathbf{q}}_\theta^{\tau_1} & \delta\tilde{\mathbf{q}}_\theta^{\tau_2} & \delta\tilde{\mathbf{q}}_\theta^{\tau_3} \\ \tilde{p}_\varphi & \delta\tilde{\mathbf{q}}_\varphi^{\tau_1} & \delta\tilde{\mathbf{q}}_\varphi^{\tau_2} & \delta\tilde{\mathbf{q}}_\varphi^{\tau_3} \\ 0 & \hat{p}_{\rho_i} & \hat{p}_{\theta_i} & \hat{p}_{\varphi_i} \end{vmatrix}. \quad (\text{A2})$$

Appendix B: Rebounds of Paraxial Rays

[25] The \mathcal{P} and \mathcal{R} operators for rebounds on a flat ground are:

$$\mathcal{P} = \begin{pmatrix} \mathcal{P}_1 & 0 \\ \mathcal{P}_2 & I_d \end{pmatrix}, \quad \mathcal{R} = \begin{pmatrix} I_d & 0 \\ \mathcal{R}_1 & \mathcal{R}_2 \end{pmatrix}; \quad (\text{B1})$$

with I_d , the identity matrix and $\mathcal{P}_1, \mathcal{P}_2, \mathcal{R}_1$ and \mathcal{R}_2 , 3×3 submatrices whose non zero coefficients are:

$$\begin{aligned} \mathcal{P}_1^{21} &= -\frac{\nabla_{\mathbf{p}} \mathcal{H}^I \cdot \mathbf{e}_\theta}{\nabla_{\mathbf{p}} \mathcal{H}^I \cdot \mathbf{e}_\rho}, \mathcal{P}_1^{31} = -\frac{\nabla_{\mathbf{p}} \mathcal{H}^I \cdot \mathbf{e}_\varphi}{\nabla_{\mathbf{p}} \mathcal{H}^I \cdot \mathbf{e}_\rho}, \\ \mathcal{P}_2^{11} &= \frac{\nabla_{\mathbf{q}} \mathcal{H}^I \cdot \mathbf{e}_\rho}{\nabla_{\mathbf{p}} \mathcal{H}^I \cdot \mathbf{e}_\rho}, \mathcal{P}_2^{21} = \frac{\nabla_{\mathbf{q}} \mathcal{H}^I \cdot \mathbf{e}_\theta}{\nabla_{\mathbf{p}} \mathcal{H}^I \cdot \mathbf{e}_\rho}, \mathcal{P}_2^{31} = \frac{\nabla_{\mathbf{q}} \mathcal{H}^I \cdot \mathbf{e}_\varphi}{\nabla_{\mathbf{p}} \mathcal{H}^I \cdot \mathbf{e}_\rho}, \\ \mathcal{R}_1^{11} &= -\frac{\Delta \nabla_{\mathbf{q}} \mathcal{H} \cdot \mathbf{e}_\rho}{\nabla_{\mathbf{p}} \mathcal{H}^R \cdot \mathbf{e}_\rho}, \mathcal{R}_1^{12} = -\frac{\Delta \nabla_{\mathbf{q}} \mathcal{H} \cdot \mathbf{e}_\theta}{\nabla_{\mathbf{p}} \mathcal{H}^R \cdot \mathbf{e}_\rho}, \\ \mathcal{R}_1^{13} &= -\frac{\Delta \nabla_{\mathbf{q}} \mathcal{H} \cdot \mathbf{e}_\varphi}{\nabla_{\mathbf{p}} \mathcal{H}^R \cdot \mathbf{e}_\rho}, \\ \mathcal{R}_2^{11} &= 1 - \frac{\Delta \nabla_{\mathbf{p}} \mathcal{H} \cdot \mathbf{e}_\rho}{\nabla_{\mathbf{p}} \mathcal{H}^R \cdot \mathbf{e}_\rho}, \mathcal{R}_2^{12} = -\frac{\Delta \nabla_{\mathbf{p}} \mathcal{H} \cdot \mathbf{e}_\theta}{\nabla_{\mathbf{p}} \mathcal{H}^R \cdot \mathbf{e}_\rho}, \\ \mathcal{R}_2^{13} &= -\frac{\Delta \nabla_{\mathbf{p}} \mathcal{H} \cdot \mathbf{e}_\varphi}{\nabla_{\mathbf{p}} \mathcal{H}^R \cdot \mathbf{e}_\rho}; \end{aligned} \quad (\text{B2})$$

with $\Delta \nabla_{\mathbf{q}, \mathbf{p}} \mathcal{H} = \nabla_{\mathbf{q}, \mathbf{p}} \mathcal{H}^R - \nabla_{\mathbf{q}, \mathbf{p}} \mathcal{H}^I$.

[26] **Acknowledgments.** Thanks to J. Guilbert and J. Vergoz for discussions, and to the reviewer for thoughtful comments. This work was

supported by CEA/DAM/DASE through grant n^o 4600020205. This is contribution Géosciences Azur n^o 754.

References

- Abdullaev, S. S. (1993), *Chaos and Dynamics of Rays in Waveguide Media*, Gordon and Breach, New York.
- Besset, C., and E. Blanc (1994), Propagation of vertical shock waves in the atmosphere, *J. Acoust. Soc. Am.*, *95*, 1830–1839.
- Burridge, R. (1976), *Some Mathematical Topics in Seismology*, Courant Inst. of Math. Sci., New York Univ., New York.
- Chapman, C. H. (1985), Ray theory and its extensions: WKBJ and maslov seismograms, *J. Geophys.*, *58*, 27–43.
- Farra, V., and R. Madariaga (1987), Seismic waveform modeling in heterogeneous media by ray perturbation theory, *J. Geophys. Res.*, *92*, 2697–2712.
- Farra, V., J. Virieux, and R. Madariaga (1989), Ray perturbation theory for interfaces, *Geophys. J. Int.*, *99*, 377–390.
- Garcés, M. A., R. Å. Hansen, and K. G. Lindquist (1998), Traveltimes for infrasonic waves in a stratified atmosphere, *Geophys. J. Int.*, *135*, 255–263.
- Hedin, A. E. (1991), Extension of the MSIS thermospheric model into the middle and lower atmosphere, *J. Geophys. Res.*, *96*, 1159–1172.
- Hedin, A. E., et al. (1991), Revised global model of upper thermosphere winds using satellite and ground based observations, *J. Geophys. Res.*, *96*, 7657–7688.
- Hedin, A. E., et al. (1996), Empirical wind model for the upper, middle, and lower Atmosphere, *J. Atmos. Terr. Phys.*, *58*, 1421–1447.
- Sutherland, L. C., and H. E. Bass (1996), Atmospheric absorption in the atmosphere at high altitudes, paper presented at 7th Long Range Sound Propagation Symposium, Ecole Cent. de Lyon, Lyon, France.
- Virieux, J., and V. Farra (1991), Ray tracing in 3-D complex isotropic media: An analysis of the problem, *Geophysics*, *56*, 2057–2069.
- Virieux, J., N. Garnier, E. Blanc, and J.-X. Dessa (2004), Paraxial ray tracing for atmospheric wave propagation, *Geophys. Res. Lett.*, *31*, L20106, doi:10.1029/2004GL020514.

J.-X. Dessa, Laboratoire de Géosciences Marines, Institut de Physique du Globe de Paris, Paris F-75252, France. (dessa@ipgp.jussieu.fr)

J. Virieux, Géosciences Azur, Université de Nice-Sophia Antipolis, Valbonne F-06560, France. (viri@geoazur.unice.fr)

S. Lambotte, EOST, Institut de Physique du Globe de Strasbourg, Strasbourg F-67084, France. (sophie.lambotte@cost.u-strasbg.fr)